Shanghai Key Laboratory for Prevention and Treatment of Bone and Joint Diseases with Integrated Chinese-Western Medicine, Shanghai Institute of Traumatology and Orthopaedics, Department of Orthopaedics, Shanghai Ruijin Hospital, Shanghai Jiaotong University School of Medicine, Shanghai, China

OIC-A006-loaded true bone ceramic heals rabbit critical-sized segmental radial defect

HUARONG SHAO, JIN SHAO, HAILIN BIAN, QIANG ZHAO, QI ZHOU, JIN QI, YAPING ZHU, JINSHENG WANG, NIANDONG QIAN, BO CHEN, LIANFU DENG

Received May 21, 2011, accepted June 16, 2011

Prof. Lianfu Deng, Shanghai Institute of Traumatology and Orthopaedics and Department of Orthopaedics, Ruijin Hospital Affiliated to Shanghai Jaotong University, 200025 Shanghai, China
lianfudeng@sina.cn

Pharmazie 67: 247–252 (2012) *doi: 10.1691/ph.2012.1072*

It has been reported that OIC-A006, an osteogenically inducible compound, is able to promote osteogenesis *in vitro* and *in vivo*. In this study, we used a rabbit critical-sized segmental radial defect model (CSD) (15 mm) to analyse the osteogenic activity of OIC-A006 in non-cell-seeded tissue engineering bone substitutes. The scaffold carrier was bovine sintered bone "true bone ceramic (TBC)". OIC-A006 was delivered by PLGA (D,L-lactide-co-glycolide acid) microspheres. Drug-free PLGA microspheres and rhBMP-2-loaded PLGA microspheres were used as negative and positive control groups, respectively. Three kinds of composite were fabricated by coupling TBC, type-I collagen and the corresponding microspheres. The animals were randomly divided into 4 groups: (1) Group A: defect only, (2) group B:TBC/Collagen/drug-free-microspheres, (3) group C:TBC/Collagen/ OIC-A006-microspheres, (4) group D: TBC/Collagen/rhBMP-2-microspheres. The samples were analysed by histology, X-ray,microcomputed tomography (μ-CT), and biomechanical analyses. The results showed that OIC-A006 promoted bone regeneration to a remarkable extent. It is suggested that the application of OIC-A006 might be a valuable method in bone tissue engineering for healing large segmental defects of long bones. However, the biomechanical strength was a little inferior to that of BMPs.

1. Introduction

Massive bone defects remain a major challenge to reconstructive surgery (DeCoster et al. 2004). Autologous bone grafting (ABG) is currently regarded as the treatment of choice. However, autogenous bone grafting also has its drawbacks. Harvesting of autogenous iliac crest bone graft is associated with many complications including nerve injury, arterial injury, and chronic long-term pain (Kurz et al. 1989). Also, the amount of autogenous bone graft available is limited in quantity, which becomes problematic for long fusions or in patients undergoing revision surgery who have had previous bone grafts harvested from the iliac crests. To avoid these disadvantages, a wide range of different artificial bone-substitute materials (BSM) have been developed over the years (Drosse et al. 2008). From the introduction of the concept of osteoinduction (Urist 1965) to the identification (Wozney et al. 1988) of bone morphogenetic protein (BMP) and to the first clinical application (Johnson et al. 1988) of BMPs, the BMP family, mainly BMP-2, BMP-4 and BMP-7, has been reported to be the most potent osteotropic factor in the promotion of bone formation, both *in vivo* and *in vitro*. One of its pivotal roles is to promote bone regeneration in synthetic bone graft substitutes (Drosse et al. 2008). However, there exists a series of problems, such as short biological half-life (Saltzman and Baldwin 1998), poor stability, safety and cost effectiveness. In addition, their activity may be compromised during the process of making a controlled delivery system with other materials. All these factors have hampered their practical clinical use, making it necessary to exploit small molecular compounds as substitutes for growth factor.

OIC-A006 (Cai et al. 2008) is a BMP-mimicking osteoinductive small-weight-molecule compound recently discovered by our team. It imitates BMPs by activating the Smed-signaling cascade to enhance bone formation *in vivo* or *in vitro*. In this study, we demonstrate the effectiveness of OIC-A006 in enhancing healing of segmental bone defects using no-cell-seeded bone tissue-engineering implants in a rabbit critical-sized radial defect model. We speculate that OIC-A006 could be used to construct bone substitute to promote large segmental defect healing in long bones.

2. Investigations and results

To evaluate the effect on the healing of rabbit critical-sized radial defects of OIC-A006-loaded TBC scaffold, we prepared TBC scaffold (Fig. 1A), and OIC-A006-loaded, OIC-A006-free and rhBMP-2-loaded PLGA (D,L-lactide-co-glycolide acid) microspheres (Fig. 1A/B). They were integrated into three kinds of composites by coupling TBC, type-I collagen and the corresponding microspheres, respectively (Fig. 1A/C/D). OIC-A006-free PLGA microspheres and rhBMP-2-loaded

Abbreviations: OIC-A006, Osteogenic inducible compound-active 006; BMPs, Bone morphogenesis proteins; BMSCs, bone marrow stem cells; CSD, Critical-sized defect.; TBC, true bone ceramic bone.

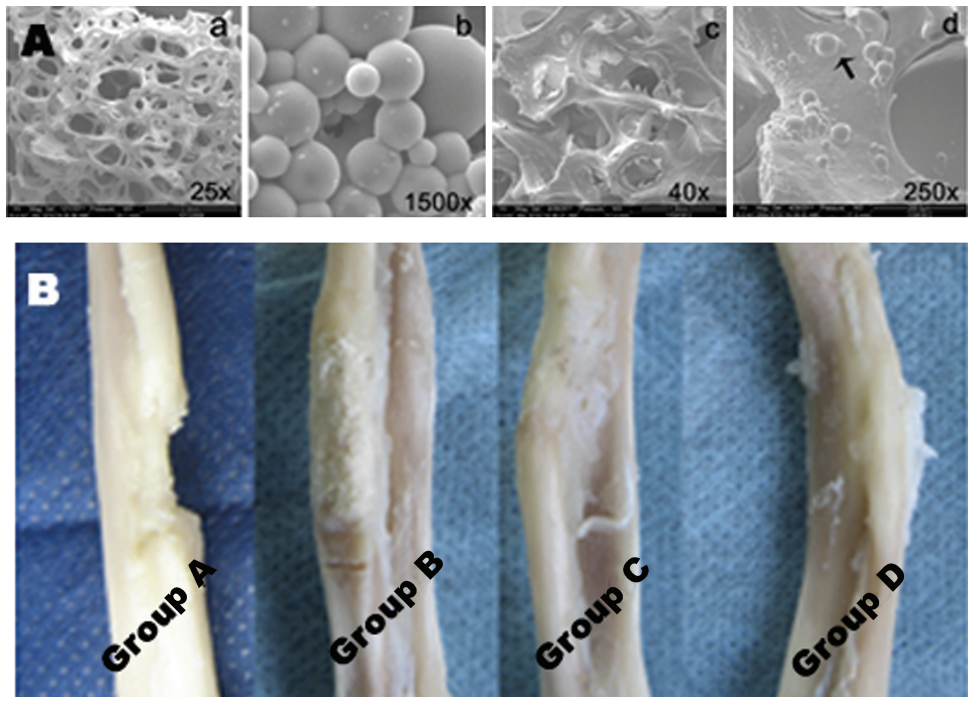

Fig. 1: A: Scanning electron microgram (SEM) of TBC (a, original magnification 25×), PLGA microspheres (b, 1500×), the retiform appearance of TBC/collagen/microspheres composites (c, 40×), and the microspheres(↑) in the composites (d, 250×). B: Representive pictures of the gross anatomy during postoperative week 12

PLGA microspheres were also prepared as negative and positive control groups, respectively. The animals were randomly divided into 4 groups: (1) Group A: defect only, (2) group B: TBC/Collagen/drug-free-microspheres, (3) group C: TBC/Collagen/OIC-A006-microspheres, (4) group D: TBC/Collagen/rhBMP-2-microspheres. Animal models were established and the composites were implanted into the defects. The samples were retrieved, and general observations, macroscopic evaluation, biomechanical analyses and quantitative analysis of histology, X-ray and microcomputed tomography (μ-CT) were made at 4, 8 and 12 weeks after surgery.

2.1. General observations and macroscopic evaluation of specimens

No bridging callus was observed in empty defects at any time point. At 4 weeks, the defects of the rhBMP-2 group were bridged by large amounts of bony callus. In the OIC-A006 group, the defects were bridged by small amounts of bony callus. The drug-free group, mainly shows fibrous-like granulation tissue during growth. At 8 weeks, bony callus increased more noticeably in the rhBMP-2 and OIC-A006 groups. At 12 weeks, the defects of rhBMP-2 group were wrapped by callus, and on the surface of samples of OIC-A006 group, the callus increased with very little of the TBC exposed, but in the drug-free group, a large part of the TBC scaffold was observed to be exposed, with only a little bony tissue generated in the region adjacent to normal bone bed (Fig. 1B).

2.2. Radiographic evaluations

In the blank group, the defects were left unbridged at any time point. The marrow cavities at both ends of the osteotomy were blocked and sclerotic at 12 weeks. In the composite-filled group, the degree of radio-opacity of the composites generally increased with time. The radio-opacity progressed faster in the OIC-A006 and rhBMP-2 groups than in the drug-free group. In the rhBMP-2 group, a bony connection was observed in the 4th week, bone remodelling clearly progressed from 8 weeks to 12 weeks (Fig. 2).

2.3. Micro-CT results

The μ-CT images show that the volume of new bone in the OIC-A006 group was obviously larger than in the drug-free group at every time point. In rhBMP-2 samples, by the 12th week the new bone was partly reabsorbed, marrow cavity had obviously formed and a perfect bony union was achieved, while no obvious medullary cavity formed in group C (Fig. 2).

Quantitative analysis showed that the volume of new bone (mm^3) in the OIC-A006 group was clearly larger than in the drug-free group ($p < 0.05$). The volume of newly formed bone in the drug-free and OIC-A006 groups increased continuously with time,while in the rhBMP-2 group, the volume of new bone reached a peak in the 8th week and then decreased gradually. This indicated that new bone regeneration and remodelling progressed earlier and faster in the rhBMP-2 group than in the OIC-A006 group (Fig. 4A).

2.4. Histological evaluation

In general, histological findings were consistent with the X-ray (Fig. 2) and μ-CT (Fig. 2) findings. Sealing-callus presented at osteotomy ends in all groups. There was more new bone formation growing into both ends of the TBC or the area adjacent to the intact ulnar bone. New bone formation in the central region of the scaffold occurred later and was less. Fusion of ulnar and radial bone was also seen in all samples. The bone formed along the surface of the TBC pores with no intervening fibrous layer. This indicates that the TBC has excellent osteoconductive properties. The presence of lymphocytes or multinucleated giant cells did not differ between groups. No inflammation reactions were observed. The area of new bone in OIC-A006 was larger than in the drug-free group. In the 12^{th} week, bone marrow tissue was observed in the central region in samples from the rhBMP-2 group. (Fig. 3). The quantitative measurements of new bone area were consistent with the μ-CT results (Fig. 4B).

2.5. Bone-labelling

The average distances between the two fluorescent mineralized lines in 8-week samples are shown in Fig. 3. The differences in

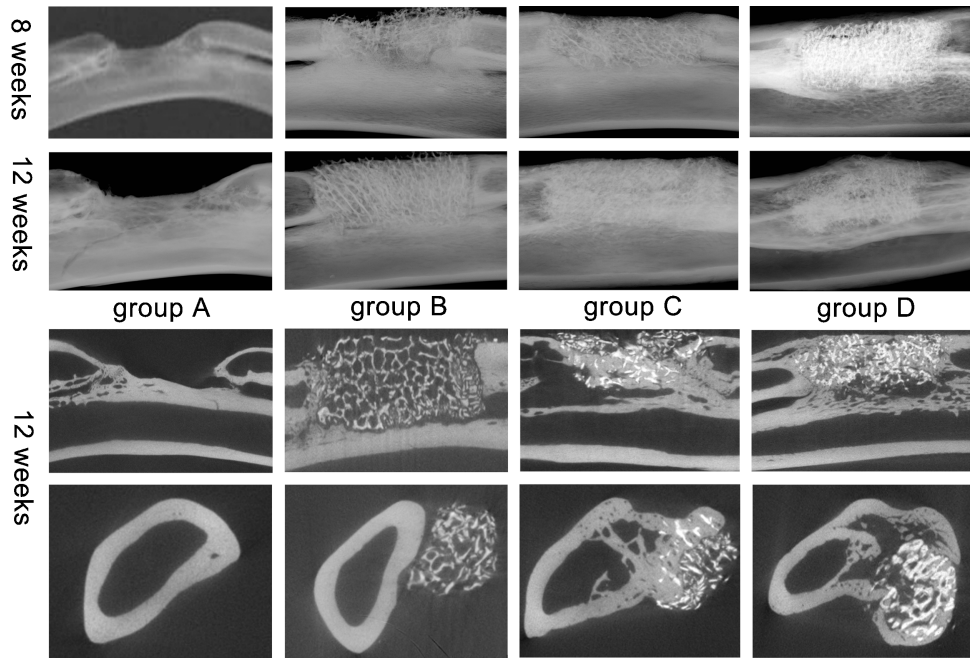

Fig. 2: Radiographs and tomograms. The panels of the top two rows were representive images of radiographs of 8 and 12 weeks. The remained defect in Group A, the increasing trend of the new bone in group C, and perfect healing in Group D (original magnification 4×). The panels of the 3th show longitudinal μ-CT tomograms and the bottom row show transverse section in the middle of the boney defect of 12 weeks samples

bone growth rate were significant between groups B, C, and D ($P < 0.05$) (Fig. 4D).

2.6. Biomechanical results

The relative stiffness of samples at 12 weeks was compared among all groups. The stiffness of samples in the OIC-A006 group was significantly higher than in group B ($p < 0.05$). Samples in the rhBMP-2 group exhibited the highest stiffness ($p < 0.05$) (Fig. 4C).

2.7. Discussion

As mentioned above, OIC-A006, a small molecule polypeptide compound, mimicking Smad1, interacts with Hox to stimulate bone formation (Cai et al. 2008; Liu et al. 2004). In our previ-

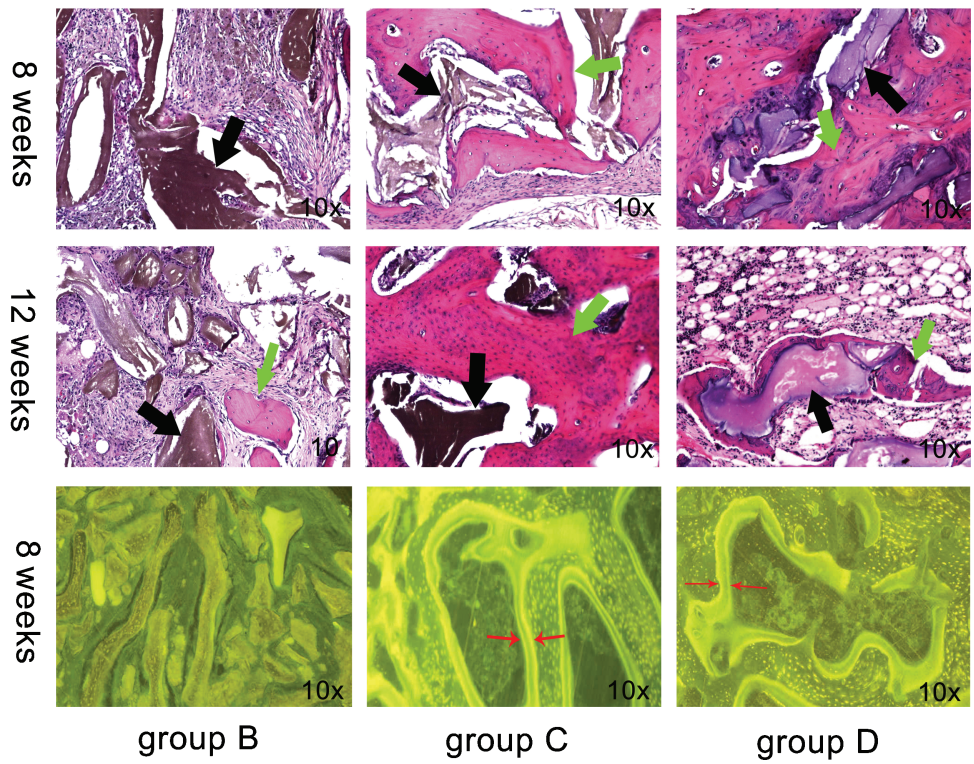

Fig. 3: Histplogyical micrograph and oxytetracycline fluorescent images. The panels of the top two rows were the representive histplogyical micrograph of the middle of the implanted composites in 8 and 12 weeks. The new bone formation in groups B, C, and D obvious, and the difference between them were significant (green arrows signal bone; black arrows signal TBC; red arrows signal marrow tissue. HE staining, original magnification 10×). The panels of the bottom row show oxytetracycline fluorescent mineralized lines in 8 weeks samples (original magnification, 10×)

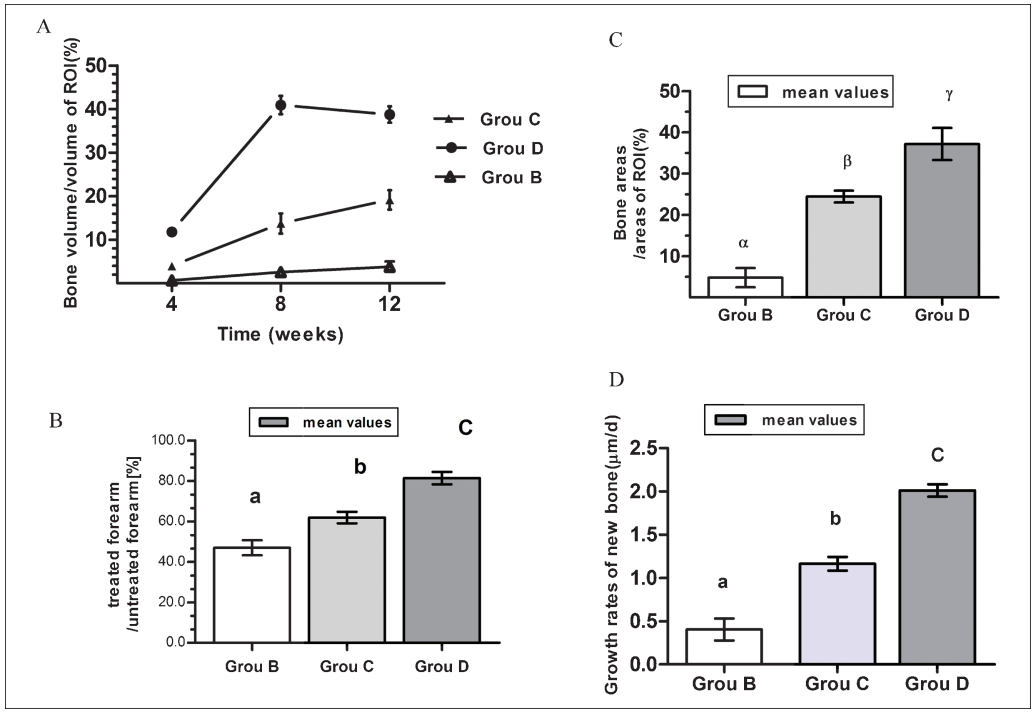

Fig. 4: Line chart and column diagram describing the amount of new bone, mechanical test and new bone growth rates. A shows quantitative analysis of new bone measured in μ-CT in samples at every time point. Diagram B shows the amount new bone on the 12th week measured in histology evaluation. C shows quantitative comparisons of bending strength on the 12th week time points and D shows the bone-labeling analysis of the 8th week samples. The rank of growth rates of new bone is group D > C > B($P < 0.05$) (Means with the same letter are not significantly different (one-way ANOVA followed by Tukey's Multiple comparison, alpha level = 0.05, group = 3, $n = 5$ for each group)

ous study, promotion of osteogenesis was observed in healing cranial critical-size defects (Cai et al. 2008). In this paper, a further study involving long bone defect healing was carried out in a rabbit radius critical-size defect model. This model has been used extensively because of its advantage of sparing internal and external fixation because the adjacent intact ulna provides stability to the created radial defect (Geiger et al. 2007). In order to avoid the influence of epiphyseal growth related to animal age, we selected seven- to nine-month-old skeletally mature rabbits, and ensured that the epiphyseal plates were closed. It was feasible using this model to evaluate the effect of the drug in promoting bone healing. The TBC as scaffold was also appropriate in healing bone defects (Katoh et al. 1993; Cestari et al. 2009). The formation of the sustained drug delivery system as a composite implant was an important aspect. OIC-A006 and rhBMP-2 containing PLGA controlled-release microspheres were prepared, ensured a precisely effective drug delivery system (Cleland 2001). Our preliminary experiments confirmed an ideal controlled-release profile of drug from this controlled-release structure (data not shown). The quantity of type-I collagen was equal in each implant. Thus, in this study, the only variable factor affecting bone regeneration was the drug. Following controlled release, this exerted an effect within and in the vicinity of the implants to promote bone formation. The bovine sintered bone, or true bone ceramic bone (TBC) possesses a similar inorganic composition and pore structure to the original cancellous bone and has good biocompatibility. It is able to support the rapid penetration of vessel ingrowth and bone formation from the host bone bed to the center of the implant (Hashizume et al. 1998), with neither immunogenicity nor cytotoxicity being observed (Minamide et al. 1999; Katoh et al. 1993). The histocompatibility and mechanical properties were further improved after coating with type-I collagen.

In this study, X-ray results are shown, but no quantitative analysis was made, because TBC is not radiolucent and the image grey level is similar to that of bone. As a general observation, a consistent trend can be observed from the image grey level. The radiographic results for the rhBMP-2 and OIC-A006 groups at 12 weeks show obvious cortical continuity. In group A, there is only sealing-callus and a little regenerated bone in the empty defect. Subsequent μ-CT and histological results confirmed what was observed in the overall view and by X-ray. As is well known, because of the two-dimensional nature of X-ray and histology examination techniques, their ability to orientate and quantify the new bone formation in and around a defect site can be limited. Fortunately, μ-CT provided three-dimensional images, which can be precisely analysed. A comprehensive analysis ensured authentic results in this study.

In μ-CT and histology quantitative analysis, new bone formation was higher at the two osteotomy ends of the radius and in the region adjacent to the ulnar bone in every group, even the non-drug group. This confirmed the pathological response to trauma, in which cells from surrounding tissue, especially from peripheral periosteum,bone marrow, and the local release of various growth factors, also play a pivotal role. In group A, because of the absence of a scaffold to provide physical support for cells, bone regeneration only took place at the two osteotomy ends and the surface of the ulnar bone. In group B,TBC played an osteoconductive role. The new bone regenerating from peripheral remnant periosteum or marrow tissue at both osteotomy ends could progress along the TBC and, with time, a small quantity of new bone even grew into the central part of the samples. Thus, the amount of new bone was larger than for the blank group. But this was limited growth, without sustaining stimulation of bone-regenerating factor.

In contrast to bone regeneration at peripheral areas of TBC, in the central region of the TBC, the cells that engage in osteogenesis mainly derive from local haematoma organization and the invasion of blood vessels. These osteogenically committed cells were mainly mesenchymal stem cells, especially bone marrow mesenchymal stem cells (BMSCs). In rhBMP-2-loaded samples, osteogenesis occurred simultaneously in core

and peripheral areas because BMPs singly induce bone development de novo from connective tissue perivascular cells or other osteoprogenitor cells (Nimni 1997). Osteogenesis also occurred simultaneously in core and peripheral areas in OIC-A006-loaded samples. In contrast, there was little new bone formation in the core of the TBC in the drug-free group (Fig. 3). This indicated the activity of the drug in inducing bone formation.

Histology sectioning (HE) and bone-labelling revealed that the process of bone formation started in the surface of the TBC scaffold and progressed away from it (Fig. 3). This indicated three aspects: (i) the good biocompatibility and conductivity of the TBC/collagen scaffold; (ii) the migration, proliferation and commitment of adjacent host cells; and (iii) the remarkable osteoinductive effect of OIC-A006 and rhBMP-2. By analysing the amount of new bone formation, bone growth rate (Figs. 3 and 4D) and the mechanical strength (Fig. 4C), an evident trend was observed that the OIC-A006 group achieved better results than the drug-free group, which was consistent with our previous research (Min et al. 2008). In the rhBMP-2 group, the decreased new bone (Fig. 4A) and bone marrow tissue formation in the central region (Fig. 3), and also the higher mechanical strength (Fig. 4C) of 12-week samples, indicated that rhBMP-2 has a greater osteoinductive capability. In short, the OIC-A006 group achieved a better healing effect than in the non-drug-loaded group, but it was still not comparable to the TBCc/rhBMP-2 group. For further verification of the osteogenic activity of OIC-A006, investigations in larger animal models, e.g. sheep, are necessary.

3. Experimental

3.1. Construction of osteoinductive bone graft substitute

3.1.1. Preparation of TBC scaffold

Following the method described in Minamide et al (1999), bovine cancellous bone blocks (5 mm × 5 mm × 15 mm) were delipidized and deproteinated, and the remaining cancellous material was sintered at 1100 °C for 3 h in a electric muffle kiln to form cuboid TBC implants. The chemical formula of TBC is $Ca_{10}(PO_4)_6(OH)_2$, which is similar to commercially available hydroxyapatite (Katoh et al. 1993). Scanning electron micrography (SEM) of the surface of TBC shows that it retains the original interconnected pore structure (Fig. 1A/a).

3.1.2. Preparation of OIC-A006-loaded and rhBMP-2-loaded PLGA controlled-release microspheres

The chemical synthesis of OIC-A006 and the preparation of drug-loaded and non-drug-loaded PLGA controlled-release microspheres were carried out in cooperation with the Shanghai Institute of Materia Medica. The molecular formula of OIC-A006 refers to M. Cai et al (2008). By solvent extraction from a W1/O/W2 dispersion, DFO/OIC-A006 and rhBMP-2 (rhBMP-2, Peprotech, 102-02) were microencapsulated by end-group uncapped 14 kDa poly(DL-lactide-co-glycolide) (PLGA, 50:50) (P2191, Sigma) with excellent encapsulation efficiency (80%). A scanning electron micrograph (SEM) of the surface is shown (Fig. 1A/b).

3.1.3. Preparation of drug-loaded and drug-free composites

The microspheres were dispersed in 150 μL type-I collagen (Sigma C3867) then dripped into TBC. Each of the OIC-A006-composites contained 6.5 mg OIC-A006 and each of the rhBMP-2-composites contained 100 μg rhBMP-2. Drug-free-composites (DFCs) consisted of TBC, type-I collagen and drug-free-PLGA. The retiform structure and the microspheres in the TBC were observed (Fig. 1A/c and d). All implants used in this study were sterilized using ethylene oxide gas.

3.2. Animal model

Seven- to 9-month-old skeletally mature male New Zealand white rabbits (NZWR) (provided by the laboratory animal center of Shanghai Institute of Traumatology and Ruijin Hospital, Shanghai Jiaotong University, China), weighing 3.2–4.6 kg, were used for the current randomized study. All the rabbits were screened for good physical condition, and epiphyseal closure was confirmed by X-ray imaging. Unilateral critical-sized defects (CSD) of the radius of the rabbits were made. The institutional Animal Care and Use Committee approved all animal experimental protocols. A total of 100 animals/defects were randomized into 4 groups (A to D). The critical-sized defects (CSD) were filled with: (1) Group A: control group (defect only), (2) group B: TBC/Collagen/drug-free-microspheres, (3) group C: TBC/Collagen/OIC-A006-microspheres, (4) group D: TBC/Collagen/rhBMP-2-microspheres.

3.3. Surgical procedure and treatment

After two weeks of acclimatization, the rabbits were operated on under anesthesia by intravenous injection of 3% pentobarbital (30 mg/kg). Under anesthesia, the left forelimb was shaved and then immobilized on the abdomen. A longitudinal incision of 3 cm was made along the radius and soft tissue was dissected after disinfecting with povidone-iodine and covered with a segregating clothing. The radius was exposed by gentle retraction of the muscles. After cutting and peeling off the periosteum *in situ*, a 15 mm segmental diaphyseal defect was created in the middle of the radius using a mini-oscillating saw under continuous saline cooling. The periosteum near the defect on each side of the remaining proximal and distal fragments of the radius, and the interosseous membrane, were also stripped and removed. The implant was pressed to fit into the defect. Muscles, fascia and skin were separately closed over the defect and no internal or external fixations were used. Each rabbit was administered 200,000U of penicillin intraoperatively and on the first postoperative day to prevent infection. Water and food were supplied *ad libitum*. Postoperative activities, food intake and wound healing were observed. At 4, 8 and 12 weeks after surgery, rabbits of each group were sacrificed and specimens were retrieved.

3.4. Evaluation and methods

3.4.1. Radiographic examination

4% PFA-fixed specimens were examined with a Fixitron X-ray apparatus (USA). Serial anterior-posterior radiographs of 4, 8 and 12-week samples were obtained. The exposure conditions were 36 kV, 6 s at 4× magnification.

3.4.2. μ-CT examination

Specimens fixed with 4% PFA were examined with a μ-CT system (GE Healthcare Explore Locus-SP, MicroView ABA 2.2, USA). The whole defect area was chosen as the region of interest (ROI) (Voxel size: 0.015 × 0.015 × 0.015, ROI type: box). A virtual box drawn in the defect was used to standardize measurements including 1.5-cm segmental defect and 0.5 mm adjacent intact bone at both ends.

To assess the amount of newly regenerated mineralized bone matrix quantitatively, the digitized data were analyzed with the GEHC MicroView ABA 2.2 software package and the amounts of newly formed bone were compared by the percentage of newly formed bone voxels of the total virtual cylinder voxels.

3.4.3. Histological examination

Samples were prepared, consisting of the 15-mm segmental defect and 5 mm of proximal and distal cortical bone with the corresponding ulna adjacent to the defect, and were then decalcified in 14% EDTA in 0.1 M Tris-FCL buffer, pH7.2 over a period of 10 weeks. The decalcified samples were hemisected sagittally through the center of the plane creating two halves and then processed through graded alcohols and xylene, and embedded with paraffin wax (Leica ASP200S, Ege 1160) in a way that the section through the half sample (radius and ulna) lay parallel to the upper surface of the embedding block. This embedding position was made the standard position in an attempt to ensure that the same region was evaluated in all specimens. Then, 3 sections (5 μm) from each sample (total 5 per group) were prepared and stained with hematoxylin and eosin (HE) to evaluate newly formed bone, fibrous tissue and TBC scaffold. The micrographic images were digitized with a software package provided by the School of Life Sciences, Shanghai Jiaotong University. Bone and bone formation were quantified from the pixels representing bone. The area occupied by bone was expressed as a percentage of the image under evaluation.

3.4.4. Bone labelling

Two series of oxytetracycline injections (Sigma T3258-5G) were given to groups B to D at the 8-week time point. A dosage of 30 mg/kg was administered via intramuscular injection. Fluorochromes were first injected 14 days and than 4 days before sacrifice. After sacrifice, the retrieved samples ($n = 5$) were dehydrated in ethanol of increasing concentration (from 70 to 100%) and then in pure acetone for 7 days and then embedded in the standardized position. Thin sections (20 μm) were prepared in the longitudinal direction using a sawing and grinding tachnique (Exakt Apparatebau, Hamburg,

Germany). The sections were examined using fluorescent light microscopy (Axiovert 200, Carl Zeiss, Germany), The two parallel fluorescent lines corresponding to the two injections of fluorochrome were observed. The measurements were performed using the Carl Zeiss Axiovision 3.1 software package. In order to minimize experimental errors resulting from the different cutting angles, 5 sites of double labelling were selected on each histological section. On each site, five measurements were taken and averaged, i.e. 25 variables were counted on each section. Three sections were measured. The bone growth rate in micrometers per day was obtained by dividing the average distance by the number of days (10 days) between the two injections (Frost 1969).

3.4.5. Biomechanical testing

A three-point bending test of the specimens at 12 weeks after surgery was performed immediately after the animal was sacrificed by means of a multifunctional mechanical tester (Type 5569, static load cell 1000N, Blue Hill Software, USA). All soft tissues were removed carefully. The radius was loaded at two points 40 mm apart on the tester with both free ends clamped horizontally, and it was confirmed that the two ends were at the same level and were coaxial. The force was applied to the samples by a controlled motion at a constant speed of 2 mm/min until rupture occurred. The bending stress δ was measured using $\delta = 8FL/pd3$, where L is the test span (40 mm), F is the bending strength load and d is the external diameter of the specimen at the breakpoint of the bone defect. Allowing for interindividual differences in bone diameter, the stiffness of each operated forearm was normalized to the stiffness of the contralateral one (in percent) by measuring the contralateral one at the same position as the operated forearm.

Acknowledgements: The authors are grateful to Shanghai Institute of Materia Medica for wholehearted cooperation to devise the small-molecule-compound OIC-A006 and the PLGA microspheres. Grants: National Natural Science Foundation of China (30872641)

References

Cai M, Liu X, Shao J, Qi J, Wang J, Zhu Y, Zhou Q, Zhao Q, Li G, Liang J, Lu WW, Deng L (2008) OIC-A006 promotes osteogenesis *in vitro* and *in vivo*. Pharmazie 63: 751–756.

Cestari TM, Granjeiro JM, de Assis GF, Garlet GP, Taga R (2009) Bone repair and augmentation using block of sintered bovine-derived anorganic bone graft in cranial bone defect model. Clin Oral Implants Res 20: 340–350.

Cleland JL, Duenas ET, Park A, Daugherty A, Kahn J, Kowalski J, Cuthbertson A (2001) Development of poly-(D,L-lactide–coglycolide) microsphere formulations containing recombinant human vascular endothelial growth factor to promote local angiogenesis. J Control Release 72: 13–24.

DeCoster TA, Gehlert RJ, Mikola EA, Pirela-Cruz MA (2004) Management of posttraumatic segmental bone defects. J Am Acad Orthop Surg 12: 28–38.

Drosse I, Volkmer E, Capanna R, De Biase P, Mutschler W, Schieker M (2008) Tissue engineering for bone defect healing: an update on a multicomponent approach. Injury 39(Suppl 2): S9–20.

Frost HM (1969) Tetracycline-based histological analysis of bone remodeling. Calcif Tissue Res 3: 211–237.

Geiger F, Lorenz H, Xu W, Szalay K, Kasten P, Claes L, Augat P, Richter W (2007) VEGF producing bone marrow stromal cells (BMSC) enhance vascularization and resorption of a natural coral bone substitute. Bone 41: 516–522.

Hashizume H, Tamaki T, Oura H, Minamide A (1998) Changes in the extracellular matrix on the surface of sintered bovine bone implanted in the femur of a rabbit: an immunohistochemical study, J Orthop Sci 3: 42–53.

Johnson EE, Urist MR, Finerman GA (1988) Bone morphogenetic protein augmentation grafting of resistant femoral nonunions. A preliminary report, Clin Orthop Relat Res 230: 257–265.

Katoh T, Sato K, Kawamura M, Iwata H, Miura T (1993) Osteogenesis in sintered bone combined with bovine bone morphogenetic protein. Clin Orthop Relat Res 287: 266–275.

Kurz LT, Garfin SR, Booth RE, Jr. (1989) Harvesting autogenous iliac bone grafts. A review of complications and techniques. Spine 14: 1324–1331.

Liu Z, Shi W, Ji X, Sun C, Jee WS, Wu Y, Mao Z, Nagy TR, Li Q, Cao X (2004) Molecules mimicking Smad1 interacting with Hox stimulate bone formation. J Biol Chem 279: 11313–1319.

Minamide A, Tamaki T, Kawakami M, Hashizume H, Yoshida M, Sakata R (1999) Experimental spinal fusion using sintered bovine bone coated with type I collagen and recombinant human bone morphogenetic protein-2. Spine 24: 1863–1870; discussion 1871-1862.

Nimni ME (1997) Polypeptide growth factors: targeted delivery systems. Biomaterials 18: 1201–225.

Saltzman WM, Baldwin SP (1998) Materials for protein delivery in tissue engineering, Adv Drug Deliv Rev 33: 71–86.

Urist MR (1965) Bone: formation by autoinduction. Science 150: 893–899.

Wozney JM, Rosen V, Celeste AJ, Mitsock LM, Whitters MJ, Kriz RW, Hewick RM, Wang EA (1988) Novel regulators of bone formation: molecular clones and activities. Science 242: 1528–1534.